Formation Considerations for Distributed Satellite SAR Systems

Thomas Kraus, Gerhard Krieger, Markus Bachmann, Alberto Moreira
Microwaves and Radar Institute, German Aerospace Center (DLR), Oberpfaffenhofen, Germany, t.kraus@dlr.de

Abstract

Distributed multichannel synthetic aperture radar (SAR) imaging is a promising concept for future Earth observation missions. The multichannel concept can mitigate the pulse repetition frequency (PRF) or minimum SAR antenna area constraints inherent to single-channel SAR systems. Thus high azimuth resolution can be maintained, while acquiring wide swathes. This significantly increases the imaging capabilities compared to current missions in terms of high spatial and temporal resolution. An important step in the design of a multi-satellite mission is the selection of an appropriate formation. Besides the driving impact on the mission objectives also safety aspects and operational requirements have to be considered. In this paper an exemplary Helix formation is analyzed and the impact of different options on the azimuth ambiguity performance is discussed.

1 Introduction

For classical single-channel SAR systems there is a limitation for the relation between resolution and swath width. This is known as the minimum antenna area constraint or the contradicting PRF requirement. Wide swathes require low PRFs whereas the broad Doppler spectrum, an inherent property of images with high azimuth resolution, calls for high PRFs to respect the Nyquist criterion. Otherwise azimuth ambiguities arise. The utilization of multiple phase centers offers the ability to reduce ambiguities and therefore acquire wide swathes with high azimuth resolution [1], [2]. Spaceborne demonstrations of the technique for single platform systems are reported in [3] and [4]. However, an extension to distributed satellite systems is even more promising. Such a system could additionally provide interferometric and tomographic capabilities [5], [6]. First results for distributed SAR imaging are reported in [7], [8], [9].

The impact of the terrain topography on the imaging performance, introduced by non-zero cross-track baselines, is discussed in [10] without addressing a specific formation flight configuration. For a multistatic SAR system different formation concepts can be envisaged as for example the Cartwheel, the cross-track Pendulum or a Helix, as discussed in chapter 2 of [11]. An important aspect when selecting a satellite formation is the avoidance of a collision, even if satellite drifts in along-track direction occur. From that point of view, the Helix formation is ideally suited as the spacecraft are permanently separated in horizontal and/or vertical direction. Since there is a lot of experience with Helix orbits from the TanDEM-X mission, this was the starting point of the analysis described in the paper at hand [12], [13], [14].

The paper is structured as follows. In section 2 the Helix formation is described and the impact of certain baseline components on the multistatic SAR data are discussed. Section 3 deals with the processing approach employed to derive the system performance and includes results for the Helix geometry and a discussion. Section 4 concludes the paper.

2 Acquisition Geometry

Selecting the formation for a multistatic mission is a key step during mission design. There are many trade-offs to be considered. On the one hand, for high-resolution SAR signal reconstruction any cross-track baseline is complicating the processing since the system gets sensitive to the topographic phase. On the other hand, interferometric or tomographic capabilities might be secondary mission goals demanding certain baselines. Additionally, safety constraints are of outmost importance.

2.1 Helix Formation

The Helix formation combines an out-of-plane (horizontal) displacement resulting from different ascending nodes with a radial separation introduced by different eccentricity vectors. Using a software tool developed for the TanDEM-X mission, an exemplary Helix formation for three satellites was designed as shown in **Figure 1**. The master satellite is assumed to be on the TerraSAR-X reference orbit whereas the slave satellites' orbits are defined by certain baseline parameters. The maximum horizontal and radial baseline is set to 150 m. The along-track baseline for a Helix formation is always twice the radial baseline. Therefore, this configuration results in along-track baselines of maximum 300 m, as shown in the top row. By setting the phase of libration of the first slave satellite to 0° and for the second one to 180°, a counter-rotating Helix can be achieved. At the bottom the perpendicular cross-track baseline and the line-of-sight (LOS) baseline are shown, assuming bistatic operation.

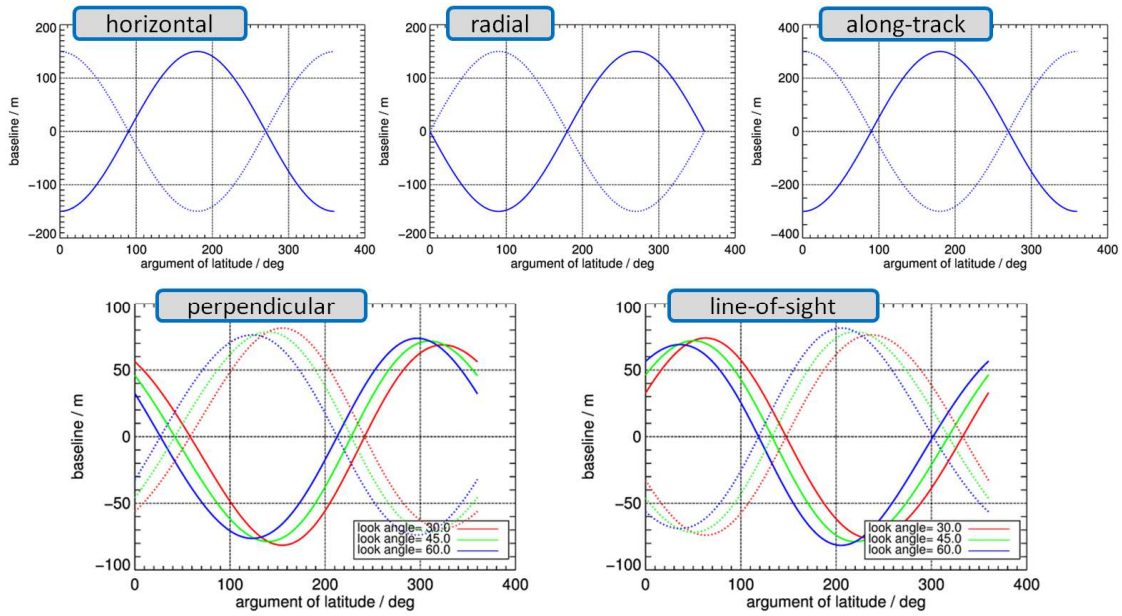

Figure 1: Horizontal, radial and along-track baseline components for an exemplary three-satellite Helix configuration (top). Effective perpendicular and line-of-sight baseline components for three different look angles (bottom). The baselines are calculated for two slave satellites shown as solid and dotted lines with reference to the master. Note, the effective perpendicular and LOS cross-track baselines are half the size of a monostatic system since bistatic operation is assumed.

2.2 Impact of the Baseline

For multichannel SAR systems on a single satellite, only the mechanically defined along-track separation of the phase centers together with the PRF and the platform velocity are of interest for the multichannel SAR signal reconstruction. These parameters determine the resulting imaging performance. For a distributed SAR system, however, the acquisition geometry is more complex. Several other factors have to be considered. An overview is given in **Figure 2**. A perpendicular baseline component $b_\perp$ leads to a range dependent interferometric phase between the channels. This is the case, even when a flat Earth model is considered as shown at the top. The center of Figure 2 discusses the impact of a topography variation in azimuth direction, which leads to an azimuth variant fringe pattern. Finally, a line-of-sight (LOS) baseline component b_{LOS} leads to different azimuth chirp rates of the signals of different channels as shown at the bottom.

In general, even if vanishing cross-track baselines are targeted for, orbit perturbations are unavoidable. The resulting baselines are demanding at least a certain mechanism to cope with the introduced sensitivity to the topography. Several processing strategies are elaborated in [10]. In section 3 the beamforming approach introduced herein is employed.

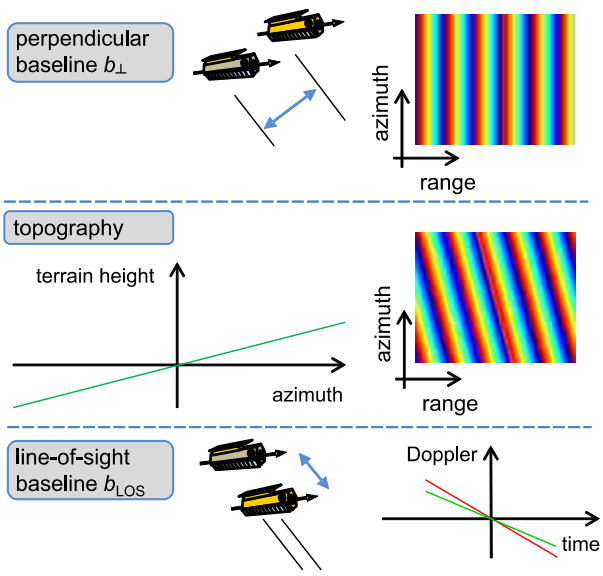

Figure 2: Effects of the distributed SAR system acquisition geometry. Perpendicular baseline $b_\perp$ leads to an interferometric phase between the channels (top). Topographic variation in azimuth direction leads to an azimuth variant fringe pattern (center). A line-of-sight component of the baseline b_{LOS} leads to different azimuth chirp rates (bottom).

3 SAR Imaging Performance

In order to evaluate the imaging performance achievable with the exemplary formation introduced in section 2.1 simulations have been conducted. **Figure 3** shows a sketch of the very flexible beamforming processing approach which is employed for this purpose [10]. The goal is to steer nulls to the positions of the ambiguities depicted in orange. Even though, this processing approach might not be the optimal one, it is able to outperform for example back-projection and Doppler domain techniques [10]. Another option would be to suppress the ambiguous power below a certain level, e.g., the noise level [15]. However, independent of the actual processing technique, the focus of the analysis described in this paper is on the variation of the ambiguity suppression performance around the orbit.

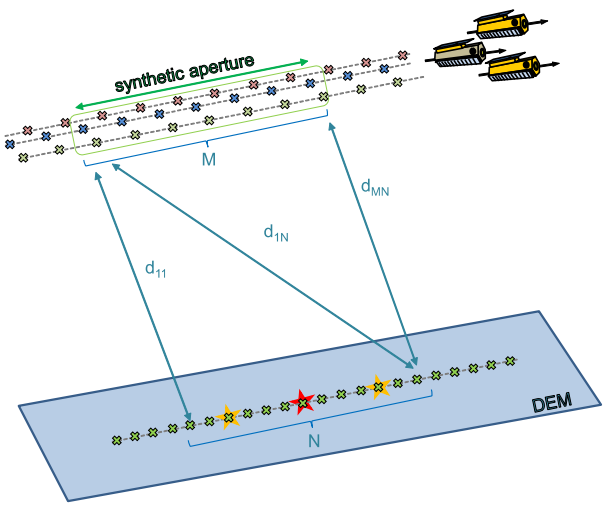

Figure 3: Sketch of the acquisition geometry and the processing for the beamforming approach for a three-channel system. The length of the synthetic aperture comprising M samples is highlighted. The distances d_{ij} of the M samples to N pixels on ground are used to calculate the beamformer weights. The target to be focused is shown in red and its ambiguities, which can also be considered as grating lobes of the beamformer, in orange.

A very important parameter for systems employing azimuth SAR signal reconstruction is the achievable azimuth ambiguity-to-signal ratio (AASR). In **Figure 4** the AASR performance for the formation given in Figure 1 is depicted over one orbit revolution of 360° argument of latitude. A topography with a slope in azimuth direction of one percent and a SAR look angle of 45° are assumed. The AASR is shown for the left and the right ambiguity of the reconstructed image separately in red and orange color, respectively. The ambiguity power is integrated on each side of the impulse response function. The blue line represents the single-channel AASR whereas the green line corresponds to a single-channel system with three times the PRF of the three-channel system under evaluation.

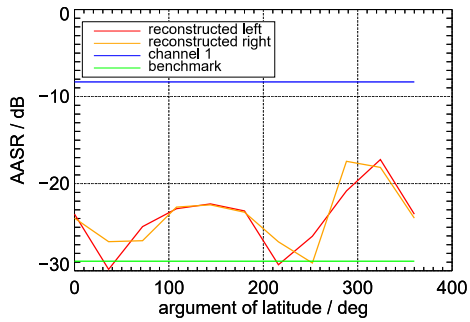

Figure 4: AASR achieved for a satellite formation as shown in Figure 1, simulated around one orbit for a look angle of 45° and an azimuth terrain slope of one percent. The sampling in along-track direction is assumed regular (ideal case). The AASR for the left and the right side of the ambiguity area is depicted in red and orange, respectively. The blue line is the AASR for a single receiver of the formation and the green line corresponds to a monostatic system with three times the PRF of the three-channel multistatic system.

The AASR of the reconstructed image varies around the orbit. At orbit positions with small perpendicular baselines (45° and 230° argument of latitude) the AASR is lower as the impact of the topography on the reconstruction is limited. However, there is a larger difference between right and left side which can be attributed to the larger LOS baseline at these positions. At orbit positions with larger perpendicular and smaller LOS baselines (around 130° and 320°) the AASR is degraded, but the ambiguity performance is more symmetric - the left and the right ambiguity have the same power.

The simulation shown in Figure 4 considers the cross-track baselines shown in Figure 1. However, it assumes a rectilinear geometry and regular azimuth sampling. As the along-track baseline for the analyzed formation is varying over ±300 m, the along-track sampling conditions are changing rapidly around the orbit. Therefore, a smaller fraction of the orbit is analyzed, respecting the along-track positions of the satellites according to Figure 1. The AASR shown in **Figure 5** is depicted over a fraction of an orbit for an argument of latitude in the range $[230°, 235°]$.

The AASR performance is highly variant due to the changing along-track sampling conditions. In **Figure 6** the sampling in along-track direction is depicted for the simulated range of the argument of latitude. The sampling is shown relative to the position under which the simulated point target for AASR assessment is seen under zero Doppler. The along-track baseline at this orbit position is in the order of 200 m as shown in Figure 1, which is small compared to the values assumed in [16]. For small baselines, the actual size of the baseline is not of major importance for the reconstruction of the azimuth signal, but the fractional relative sample spacing between the channels is still a critical parameter.

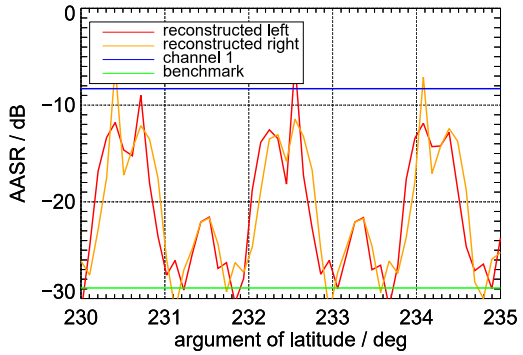

Figure 5: AASR achieved for a satellite formation as shown in Figure 1, simulated for a fraction of an orbit for argument of latitude in the range $[230°, 235°]$, for a look angle of 45° and an azimuth terrain slope of one percent. The azimuth sampling is in accordance with the along-track baseline depicted in Figure 1. The AASR for the left and the right side of the ambiguity area is depicted in red and orange, respectively. The blue line is the AASR for a single receiver of the formation and the green line corresponds to a monostatic system with three times the PRF of the three-channel multistatic system.

The spatial samples of the master satellite are depicted in blue, whereas the slave satellites' samples are shown in red and green. The spacing of the samples of the individual channels is 3.8 m, as expected for a PRF of 2000 Hz at a satellite velocity of 7600 m/s. The thin vertical orange lines indicate the positions for a regular sampling with three times the PRF, which is the optimum sampling condition for a three-channel system.

Due to the changing along-track baselines, the sampling conditions in along-track also change periodically. At an argument of latitude of approximately 230.5° the samples of all three channels are coinciding. Therefore, the slave channels cannot contribute valuable additional information and so the AASR performance is very limited as shown in Figure 5. For an argument of latitude of approximately 231.0°, however, the sampling conditions are close to ideal, which directly results in an AASR well below -25 dB. The sampling situation with three spatially coinciding channels can be regarded as the worst-case for an absolutely symmetric formation. Already shifting one of the slave satellites by, e.g., 1 m in along-track, while keeping the rest of the formation parameters constant, avoids the situation of three coinciding samples around the full orbit.

The results shown in Figure 5 are assuming a constant PRF operation. Obviously, the assumed PRF is ideal for some orbit positions, but not for others. Therefore, an operational scheme could employ a cyclic variation of the PRF in order to achieve adequate sampling conditions, assuming the along-track baseline is predictable with sufficient accuracy to command the acquisitions with a tailored PRF.

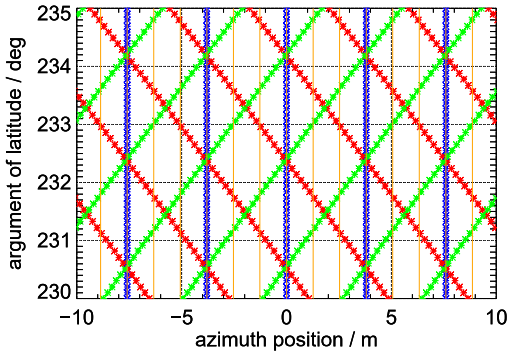

Figure 6: Along-track sampling conditions for a fraction of an orbit for arguments of latitude in the range $[230°, 235°]$. The blue samples correspond to the master channel, whereas the red and the green samples originate from the slave satellites. The orange lines highlight the positions for a regular sampling in along-track.

Concentrating on an interval of arguments of latitude of $[230°, 232°]$, where the sampling patterns are approximately repeating, a numerical search was conducted in order to find PRFs around the previously assumed 2000 Hz which provide appropriate sampling conditions. In **Figure 7** those PRFs are reported. The corresponding AASR performance is shown in **Figure 8**. The AASR for the three-channel system stays well below -25 dB, while the performance of the single-channel and the benchmark system are slightly varying, because the PRF-change is also noticeable here. It has to be noted, that the necessary change in the PRF over a range of 50 Hz is very small. Therefore, the necessary PRF variation in order to achieve good AASR is not expected to cause problems with respect to the timing of acquisitions. In the case shown in Figure 8 the symmetry of the assumed Helix formation was beneficial, because it is facilitating the search for an appropriate PRF for the three-channel system.

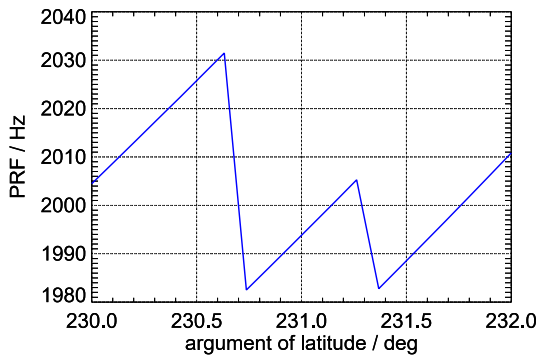

Figure 7: PRFs providing a close-to-uniform sampling for a range of arguments of latitude of $[230°, 232°]$.

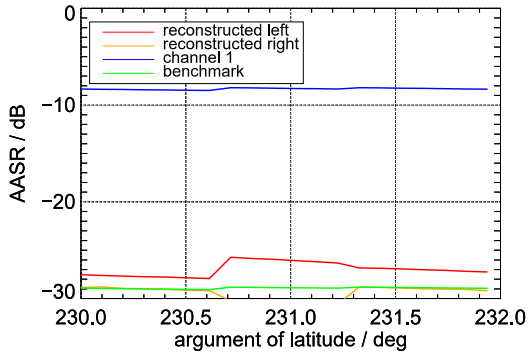

Figure 8: AASR achieved for a satellite formation as shown in Figure 1, simulated for a fraction of an orbit for argument of latitude in the range [230°, 232°], for a look angle of 45° and an azimuth terrain slope of one percent. The azimuth sampling is in accordance with the along-track baseline depicted in Figure 1, assuming a PRF as shown in Figure 7.

The search for an appropriate PRF for an adequate spatial sampling not only has to consider the satellite formation, but also the operational mode. For a satellite constellation operating in monostatic mode the sampling for each channel can be adjusted independently offering great flexibility [17], [9]. For a system operating in bistatic mode with one transmitter and several receivers, like we assumed in this paper, the sampling is driven by the PRF and the baselines between the channels. Here an optimization is necessary in order to achieve a sampling as close as possible to the uniform one. A system operating in MIMO mode with several transmitters and receivers requires an even more sophisticated optimization in order to find an appropriate pulse transmission scheme.
Another measure to avoid reduced reconstruction performance would be to invest in more channels, which would offer greater flexibility and robustness. If two channels are sampling at coincident azimuth positions at some orbit position, an additional channels' information can close the gap.

4 Summary

The paper addresses the formation selection for distributed satellite systems, focusing on the ambiguity performance for a system requiring high azimuth resolution and therefore, an azimuth signal reconstruction technique. For the simulations shown here a beamforming approach is employed and the AASR performance around one orbit revolution is shown. The performance varies around the orbit as the perpendicular and the line-of-sight baselines change. Additionally, the relative along-track motion of the satellites, an inherent feature of a Helix formation, leads to a variation of the along-track sampling conditions. For a system with constant PRF, this leads to coinciding spatial samples of the different channels at specific orbit positions. Adapting the PRF in order to achieve optimized sampling conditions re-establishes the expected ambiguity performance gain for the given satellite formation. This time-variant PRF scheme and an investment in more channels are discussed. More sophisticated techniques, like a cyclically changed or staggered PRF variation and the assessment of a random PRF scheme could be target of future research.

References

[1] G. Krieger, N. Gebert, and A. Moreira, "Unambiguous SAR signal reconstruction from nonuniform displaced phase center sampling," *IEEE Geosci. Remote Sens. Lett.*, vol. 1, no. 4, pp. 260–264, 2004.

[2] N. Gebert, G. Krieger, and A. Moreira, "Digital beamforming on receive: Techniques and optimization strategies for high-resolution wide-swath SAR imaging," *IEEE Trans. Aerosp. Electron. Syst.*, vol. 45, no. 2, pp. 564–592, 2009.

[3] J.-H. Kim, M. Younis, P. Prats-Iraola, M. Gabele, and G. Krieger, "First spaceborne demonstration of digital beamforming for azimuth ambiguity suppression," *IEEE Trans. Geosci. Remote Sens.*, vol. 51, no. 1, pp. 579–590, 2013.

[4] D. Cerutti-Maori, I. Sikaneta, J. Klare, and C. H. Gierull, "MIMO SAR processing for multichannel high-resolution wide-swath radars," *IEEE Transactions on Geoscience and Remote Sensing*, vol. 52, no. 8, pp. 5034–5055, 2014.

[5] G. Krieger and A. Moreira, "Potential of digital beamforming in bi-and multistatic SAR," in *Geoscience and Remote Sensing Symposium, 2003. IGARSS'03. Proceedings. 2003 IEEE International*, vol. 1. IEEE, 2003, pp. 527–529.

[6] ——, "Spaceborne bi- and multistatic SAR: potential and challenges," *Proc. Inst. Elect. Eng.—Radar, Sonar, Navigat.*, vol. 153, no. 3, pp. 184–198, 2006.

[7] T. Kraus, B. Bräutigam, M. Bachmann, and G. Krieger, "Multistatic SAR imaging: First results of a four phase center experiment with TerraSAR-X and TanDEM-X," in *Proc. EUSAR*, Hamburg, Germany, 2016.

[8] T. Kraus, M. Bachmann, L. Heiderich, G. Krieger, and A. Moreira, "Multistatic SAR imaging: Comparison of simulation results and experimental data," in *Proc. Inst. Elect. Eng.—Radar, Sonar, Navigat.* IET, 2017.

[9] T. Kraus, G. Krieger, M. Bachmann, and A. Moreira, "Spaceborne demonstration of distributed SAR imaging with TerraSAR-X and TanDEM-X," *IEEE Geoscience and Remote Sensing Letters*, vol. 16, no. 11, pp. 1731–1735, 2019.

[10] T. Kraus, M. Bachmann, G. Krieger, and A. Moreira, "Addressing the terrain topography in distributed SAR imaging," in *Proc. Inst. Elect. Eng.—Radar, Sonar, Navigat.*, 2019.

[11] M. D'Errico, *Distributed space missions for earth system monitoring*. Springer Science & Business Media, 2012, vol. 31.

[12] A. Moreira, G. Krieger, and J. Mittermayer, "Satellite configuration for interferometric and/or tomographic remote sensing by means of synthetic aperture radar (SAR)," 2002, U.S. Patent 6 677 884, U.S. Off. Pat. Office, Washington, DC.

[13] G. Krieger, A. Moreira, H. Fiedler, I. Hajnsek, M. Werner, M. Younis, and M. Zink, "TanDEM-X: A satellite formation for high-resolution SAR interferometry," *IEEE Trans. Geosci. Remote Sens.*, vol. 45, no. 11, pp. 3317–3341, 2007.

[14] S. D'Amico and O. Montenbruck, "Proximity operations of formation-flying spacecraft using an eccentricity/inclination vector separation," *Journal of Guidance, Control, and Dynamics*, vol. 29, no. 3, pp. 554–563, 2006.

[15] H. L. Van Trees, *Optimum array processing: Part IV of detection, estimation, and modulation theory*. John Wiley & Sons, 2004.

[16] N. Sakar, M. Rodriguez-Cassola, P. Prats-Iraola, and A. Moreira, "Azimuth reconstruction algorithm for multistatic sar formations with large along-track baselines," *IEEE Transactions on Geoscience and Remote Sensing*, vol. 58, no. 3, pp. 1931–1940, 2019.

[17] J. P. Aguttes, "The SAR train concept: An along-track formation of SAR satellites for diluting the antenna area over n smaller satellites, while increasing performance by n," *Acta Astronautica*, vol. 57, no. 2, pp. 197 – 204, 2005.